GaN Nanowire *n-i-n* Diode Enabled High-Performance UV Machine Vision System

Haitao Du, Yu Zhang, Junmin Zhou, Jiaxiang Chen, Wenbo Ye, Xu Zhang, Qifeng Lyu, Hongzhi Wang, Kei May Lau, *Life Fellow, IEEE*, and Xinbo Zou, *Member, IEEE*

***Abstract*—Machine vision as an essential component of artificial intelligence poses a significant influence on dimension measurement, quality control, autonomous driving, and so on. In this study, a high-performance ultraviolet (UV) imaging and detection system enabled by Gallium Nitride (GaN) nanowire (NW) n-i-n photodetector (PD) is presented. Based on supreme optoelectronic properties of the NW, including high responsivity of 5098 A/W, a low dark current of 4.88 pA and a photo-to-dark current ratio of 1223, machine vision system composed of a GaN NW array could achieve an accuracy of 96.21%. Furthermore, feasibility of artificial neural network (ANN) and convolutional neural network (CNN) in such a machine vision system is discussed, featuring dim and noisy environment. The visualization process shows that the superiority of CNN over ANN in image recognition is attributed to the capability of extracting spatial information and characteristics. The research results provide important insight into the development of both sensors and algorithms for machine vision systems based on GaN NW PD, inspiring further investigation into UV image detection and other areas of artificial intelligence.**

***Index Terms*—Gallium Nitride (GaN), nanowire (NW), machine learning, artificial neural network (ANN), convolutional neural network (CNN).**

I. Introduction

RECENTLY, machine vision that enables automatic object inspection and analysis has received extensive research interest [1]. Driven by artificial intelligence algorithms, machine vision systems play a significant part in a variety of fields, including autonomous driving, defect detection, and so on [2], [3]. Due to the steady advance of optoelectronic devices, machine vision system has gained dramatic progress. For example, a machine vision system based on a two-dimensional MoS_2 phototransistor array shows promising potential to overcome the von Neumann bottleneck of conventional silicon technology [4]. Based on machine learning algorithm, Mennel et al. [5] presented a photodiode array, which could simultaneously sense and process images projected onto the chip. Zhu et al. [6] reported a flexible optoelectronic sensor array that combined carbon nanotubes and $CsPbBr_3$-QDs, reaching an image recognition accuracy of 95%. There has been an increasing demand to extend the machine vision systems to ultraviolet (UV) region, enabling non-destructive and accurate detection for surface damage inspection, forest fire detection and many other fields [7], [8]. Towards that goal, UV image sensors play an indispensable role as the "eyes" of the UV machine vision system [9], [10], [11]. Nevertheless, the applications of conventional UV sensors, such as silicon photodiodes and ZnO photodiodes [12], were limited by low responsivity, high dark current and other defects, making it challenging to grasp precise information in dim scenarios. Recently, a handful of methods to improve responsivity and minimize dark current have been reported [13], [14], [15]. However, these methods faced considerable hardware and software complexity. A more reliable and efficient solution for UV image sensors suitable for dim environments is therefore highly desirable [16], [17].

Gallium Nitride (GaN) has demonstrated considerable promise for UV region due to its direct bandgap (3.40 eV), high selectivity of UV light over visible light, and high temperature stability [18], [19], [20]. Yang et al. [21] reported GaN nanobelt with responsivity > 575 A/W and dark current of 1.75 pA by buffer layer removal. Dubey et al. [22] fabricated an epitaxial single-crystalline Al film on GaN to form a UV photodetector (PD), achieving a responsivity of 670 A/W. GaN nanowire (NW) PD also received extensive research attention, owing to high responsivity, low dark current, and fast response speed [23], [24]. Kumar et al. [25] reported high responsivity of 5.1×10^3 A/W from a long GaN NW. Wang et al. [26] showed that a back-to-back Schottky contact NW could exhibit responsivity of 5.5×10^3 A/W and dark current of 10 nA. Despite the rapid progress of GaN NW PD, its potential in implementing machine vision systems is still yet to be assessed and reported.

When implementing a machine vision system, there are typically two main machine vision algorithms, namely convolutional neural network (CNN) and artificial neural network (ANN) [27], [28]. CNN is built upon convolutional layers as its essential component, enabling the network to effectively capture and extract

Manuscript received 23 April 2024; accepted 10 June 2024. Date of publication 19 June 2024; date of current version 1 July 2024. This work was supported in part by the ShanghaiTech University Startup Fund under Grant 2017F0203-000-14, in part by the National Natural Science Foundation of China under Grant 52131303, in part by the Natural Science Foundation of Shanghai under Grant 22ZR1442300, and in part by Chinese Academy of Sciences (CAS) Strategic Science and Technology Program under Grant XDA18000000. The review of this article was arranged by Associate Editor Prof. C. Teuscher. *(Corresponding author: Xinbo Zou.)*

Haitao Du, Yu Zhang, Junmin Zhou, Jiaxiang Chen, Wenbo Ye, and Xinbo Zou are with the School of Information Science and Technology, ShanghaiTech University, Shanghai 201210, China (e-mail: zouxb@shanghaitech.edu.cn).

Xu Zhang and Qifeng Lyu are with the Department of Electronic and Computer Engineering, Hong Kong University of Science and Technology, Kowloon, Hong Kong.

Hongzhi Wang is with the State Key Laboratory for Modification of Chemical Fibers and Polymer Materials, College of Materials Science and Engineering, Donghua University, Shanghai 201620, China.

Kei May Lau is with the Division of Emerging Interdisciplinary Area, Hong Kong University of Science and Technology, Hong Kong.

Digital Object Identifier 10.1109/TNANO.2024.3416509

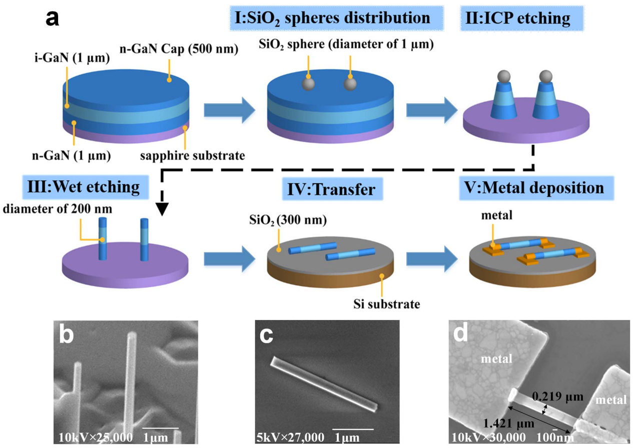

Fig. 1. (a) Process flow schematic of n-i-n GaN NW PD. (b) Corresponding scanning electron microscope (SEM) images of Single NW. (c) NW was transferred to Si substrate with a thickness of 300 nm SiO_2 on the surface. (d) The structure of the device after 500 °C annealing for 60 s.

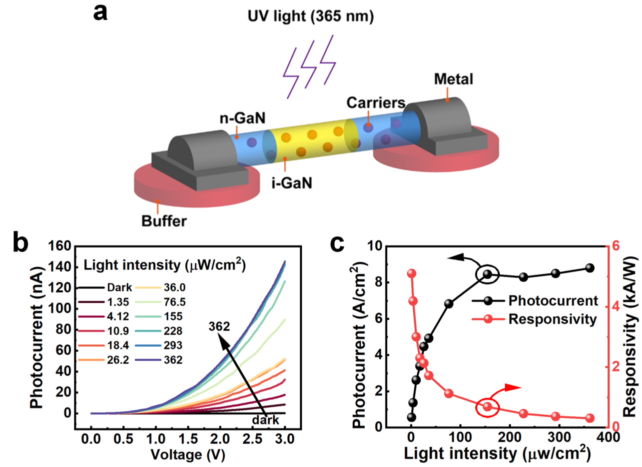

Fig. 2. (a) Schematic diagram of GaN NW generates photocurrent after irradiating by UV light. (b) Photocurrent of the GaN NW PD with different UV intensity and dark conditions. The applied voltage was from 0 to 3 V, and the UV intensity was from 0 to 362 μW/cm^2. (c) Photocurrent density and responsivity of GaN NW PD with different UV intensity at a bias of 1 V.

features from input images. ANN consists of an interconnected network of artificial neurons in layer structures that provide the capability of learning from input information through neuron layers. For instance, Zhou et al. [29] demonstrated a UV visual system based on optoelectronic resistive random access memory synaptic devices and used ANN for image recognition that achieved 98% accuracy after 2000 training epochs. However, the feasibility of UV machine vision systems based on GaN NW PD and machine learning algorithms is not established. Additionally, a detailed comparison between ANN and CNN for UV image detection is still missing, especially in low light intensity and noisy environments.

In this paper, we report a high-performance machine vision system enabled by GaN NWs array, which were obtained by a "top-down" fabrication process. Direct-current and photoelectric characteristics of GaN NW were explored. Besides, the machine vision systems implemented by CNN and ANN machine-learning algorithms was explicitly investigated, respectively. The characteristics of the two algorithms at different conditions were also compared, and the recognition results were discussed, particularly in noisy and dim environments. The characteristics of NW and detection capability indicate that GaN NW PDs, together with CNN algorithm exhibit great potential for image auto-analysis in UV environment.

II. Fabrication and Characteristics

Fig. 1(a) schematically shows the fabrication process of GaN NW PD, using a "top-down" etching method [30]. The starting GaN n-i-n thin film was grown on a sapphire substrate using metal–organic chemical vapor deposition (MOCVD) [31]. The n-i-n epitaxial layer consisted of a 1 μm Si doped n-GaN layer (doping concentration of 5×10^{18}/cm^3), a 1 μm undoped i-GaN layer, and a 500 nm Si doped n-GaN (doping concentration of 5×10^{18}/cm^3). Then Silica spheres with a diameter of 1 μm were distributed on the surface of the n-i-n structure GaN wafer as mask of the inductive coupled plasma (ICP) etching. The sample was etched in ICP system to get a nanopillar. Then the sample was put into the KOH base solution to decrease the diameter of NWs and smoothen the surface via wet etching. Fig. 1(b) displays the scanning electron microscope (SEM) images of a single NW after dry and wet etching. The NWs were removed from the sapphire substrate by sonicating in de-ionized water. Thus the NWs were transferred to the surface of 300 nm SiO_2/Si substrate and the corresponding SEM image is shown in Fig. 1(c). The NW PD device was finally fabricated by depositing metal on the both ends of the NW. The metal electrodes of NWs were patterned by e-beam lithography (EBL) and 80/80 nm Ti/Au stack metal was deposited. Then, the sample was annealed at 500 °C for 60 s to improve the contact between metal and nanowire. Fig. 1(d) shows the n-i-n GaN NW PD used in this study. The "top-down" technology could well reserve the doping profile of the original film and facilitate fabrication of NWs with better uniformity, which is beneficial for sensor array [32], [33].

Fig. 2(a) illustrates the schematic of GaN NW sensor operating with UV illumination. Fig. 2(b) displays the photocurrent curves with different UV illumination intensities and bias voltage at a wavelength of 365 nm. With enhanced UV illumination intensity, a higher photocurrent of GaN NW can be obtained, while the maximum photocurrent reached 145 nA at $V_{bias} = 3$ V for an illumination intensity of 362 μW/cm^2. The photo-to-dark current ratio (PDCR) is given by I_{UV}/I_{dark}, where I_{UV} and I_{dark} represent the photocurrent and the dark current, respectively. When GaN NW was exposed to light intensity of 362 μW/cm^2, a PDCR of 1223 was extracted at a bias of 1 V. Fig. 2(c) shows the photocurrent density and responsivity of the NW PD as a function of light intensity at $V_{bias} = 1$ V. The photocurrent increases as the light intensity increases. When the UV intensity reaches 362 μW/cm^2, the photocurrent density tends to be stable, with a maximum photocurrent density of 10.80 A/cm^2. In addition, a decrease in responsivity is observed with increasing light intensity, which is related to the increase in carrier recombination rate at high incident light intensities

TABLE I
COMPARISON OF PHOTOELECTRICAL CHARACTERISTICS WITH PREVIOUS WORKS

PDs structure	Detection wavelength(nm)	Responsivity (A/W)	Dark current (pA)	PDCR	Reference
GaN NW	360	50.25@ 1V	N.A.	N.A.	[35]
Ga_2O_3/GaN NW	248~379	753.2@ 5V	0.0542@ -5V	N.A.	[36]
Zn_2GeO_4 NW	265	5110@ 1V	N.A.	10	[37]
Ga_2O_3 PD	254	0.1@ 40V	12@ 40V	5	[38]
Si PD	635~850	0.037@ -0.5V	100@ -0.5V	N.A.	[39]
AlGaN NW	266	0.95@ -4V	6220@ -4V	500	[40]
GaN NW	365	5098@ 1V	4.88@ 1V	1223	This work

[34]. A maximum responsivity at the 1 V bias was measured to be 5098 A/W with a light intensity of 1.35 μW/cm^2. Such high responsivity is mainly due to the large photoconductive gain resulting from the long lifetime of excess electron and the electron-hole spatial separation induced by strong surface band bending in the NW [41], [42].

Table I summarizes the performance comparison of GaN NW PD in this work with those of previously reported contributions. With a similar incident wavelength, the PD in this study showed significantly higher responsivity compared with GaN NW and Ga_2O_3/GaN NW [35], [36]. The comparison also reveals that the GaN NW PD in this work demonstrates a lower level of dark current than the one from Ga_2O_3 and Si PD [38], [39], which is mainly due to the low surface state density [43]. In addition, the GaN NW in this work exhibits a much larger PDCR compared to Zn_2GeO_4 NW and AlGaN NW [37], [40]. These data show that GaN PD in this study has excellent sensitivity, and low dark current, minimized quiescent power, justifying its feasibility for UV image detection, especially in dim environments.

III. IMPLEMENTATION OF MACHINE VISION SYSTEM

Fig. 3 illustrates the complete implementation process of a machine vision system based on GaN NW PDs, including training models, image perception, and recognition. As shown in Fig. 3(a), the UV sensor array consisting of identical 28 × 28 GaN NWs was simulated to capture the input image of the object. The 365 nm UV light passed through the object with a hollow pattern, such as the digit "3", and the UV sensors array can receive the light signal to generate photocurrent. Each NW receives an optical signal from the projection and generates a photocurrent of different amplitude, corresponding to the pixel value of the object. Then the machine vision system could capture and reconstruct the object for recognition, and particularly in this study digital number is used for analysis. Fig. 3(b) and (c) show the structures of CNN and ANN training models. Both machine learning algorithms could analyze the signal and obtain the final result of the recognition process. The Modified National Institute of Standards and Technology (MNIST) was chosen as the training and validation dataset to assess the recognition accuracy of GaN NWs UV machine vision system. 60000 images of "0" to "9" are used to train the recognition model and another 10000 images are employed for testing. During the training process, the hyperparameters were also optimized, such as the number of neurons in ANN, convolution kernel and pooling kernel size in CNN according to the feedback from accuracy and loss during the training

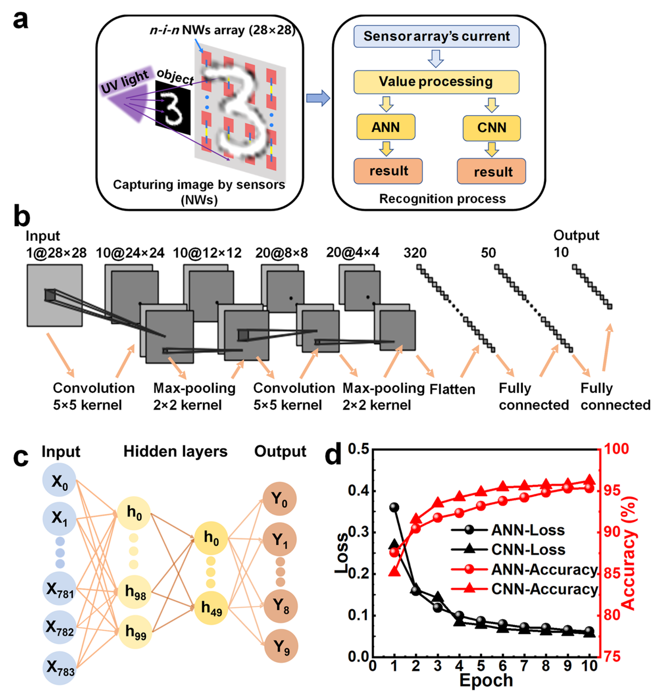

Fig. 3. Structure of a machine vision system based on the GaN NWs array. (a) The NWs array captures photo signals from the projection of pattern "3", and converts it into an electron signal. After processing data from the sensor array, ANN and CNN would output the final result, respectively. A total of 60000 images for "0" to "9" are used to train the recognition model and 10000 images to test. (b) The architecture of CNN consists of convolutional layers, pooling layers, and fully connected layers. (c) ANN consists of an input layer, two hidden layers, and an output layer. (d) The recognition accuracy and loss versus the number of training epochs from 1 to 10, both for ANN and CNN. Red and black lines represent the accuracy and training loss, respectively.

epochs. Fig. 3(d) depicts the accuracy and loss as a function of training epochs. As the number of training epochs increased, the recognition accuracy was improved and training loss was decreased. The recognition accuracy was greatly improved after only three epochs, together with a significantly reduced training loss. After ten epochs, the test accuracy and training loss for CNN reach 96.35% and 0.0569, respectively, while ANN model has slightly lower accuracy of 95.33% and slightly higher train loss of 0.0618. The results show that both CNN and ANN have a fairly outstanding ability to detect objects after ten epochs of training.

Fig. 4(a) demonstrates the binarized images of the digit "3", by definition the binarization threshold value was set to a specific gray-level (4 to 255). From the photocurrent with UV intensities

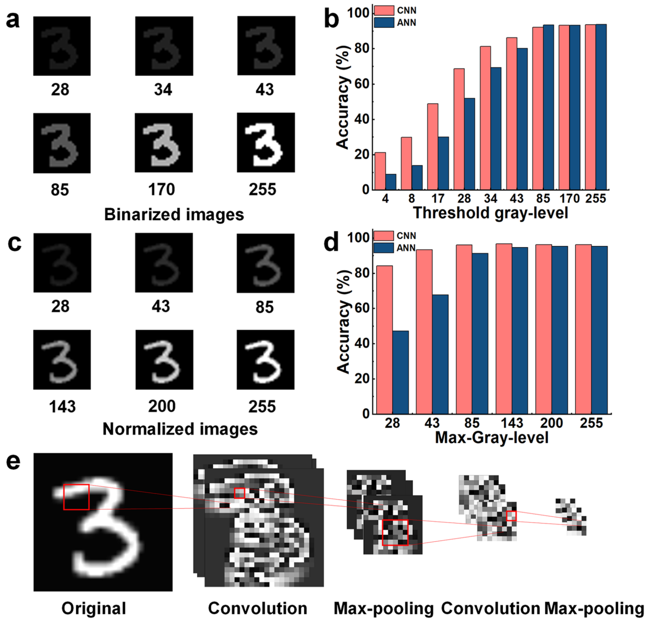

Fig. 4. (a) Binarized images of digit "3" at different none-zero gray-level, where binarization means that the non-zero gray-level is set to a specific value while others are 0 (b) Binarized image recognition accuracy versus gray-level. (c) Normalized images of different Max-Gray-level. The normalization law is that the photocurrent I = 50 nA (light intensity = 26.2 μW/cm^2) was defined to represent the gray-level of 255 and I = 8.76 nA (light intensity = 1.35 μW/cm^2) represented the gray-level of 0. (d) Normalized image recognition accuracy versus Max-gray-level. (e) Processing visualization for CNN imaging recognition, the high-dimension features of the original image are extracted by convolution layers and Max-pooling layers.

in Fig. 2(b), we defined the light intensity = 362 μW/cm^2 at which the photocurrent becomes saturated, corresponding to gray value 255 and the light intensity = 1.35 μW/cm^2 represents the gray level of 0. In the simulation of machine vision system, all GaN NWs were subjected to $V_{\mathrm{bias}} = +1$ V. Fig. 4(b) demonstrates the recognition accuracy of CNN and ANN models on binarized images (10000 testing images). At low light intensity (4.12 μW/cm^2, threshold gray-level = 4), the CNN model achieved higher recognition rates (21.34%) than the ANN model (8.92%), while at high intensity (121.57 μW/cm^2, threshold gray-level = 85) both models achieved similar accuracies (about 93%). At elevated light intensities, the recognition accuracy remains saturated. It is possible to distinguish objects with simple shapes by binarizing the image signal, but this strategy falls short when trying to identify objects with complicated shapes. Normalization was then utilized to recognize the complex images, where all gray-level values were mapped from 0 to the maximum possible value, which was from 28 to 255 in this study. Considering the linearity for normalization, the linear fitting was performed on characteristic curves at 1.35-26.2 μW/cm^2 with a coefficient of determination (COD) of 0.98 in this study. In this case, the photocurrent = 3.03 nA (light intensity = 26.2 μW/cm^2) was defined to represent the gray-level of 255 and photocurrent = 0.37 nA (light intensity = 1.35 μW/cm^2) represented the gray-level of 0 [44]. Fig. 4(d) shows the recognition accuracy with different normalized images. The accuracy of CNN was significantly higher than ANN on low Max-Gray-level (< 85) images and achieved 84.29% in dim environments (Max-Gray-level = 28, light intensity = 4.11 μW/cm^2) compared to ANN's 47.17%. In comparison to the 93% accuracy for binary images, the highest accuracy for normalized images of CNN was 96.21% and ANN was 95.29%. These results indicate that CNN well outperforms ANN at low light intensities, whereas the two models show similar capability at high light intensities [45]. Fig. 4(e) depicts the feature visualization for CNN imaging recognition. After a convolutional layer, the photocurrent matrix generated by NWs array was reduced from a size of 28 × 28 to 24 × 24, and the convolutional kernel could extract high-dimension features from the image. Then the Max-pooling layer was employed to improve the computational efficiency and to avoid overfitting by down-sampling. Despite the images have been highly abstracted to the point where they are unrecognizable to humans, it is still possible for computers to acquire features from them. The visualization process has shown the superiority of CNN over ANN in image recognition. The superiority is mainly due to CNN's convolutional kernels, which could effectively extract features and spatial information. On the contrary, the data for ANN is required to convert 2D image pixels into one-dimensional form, resulting in a lack of spatial information and an excessive increase in vector dimensionality [46].

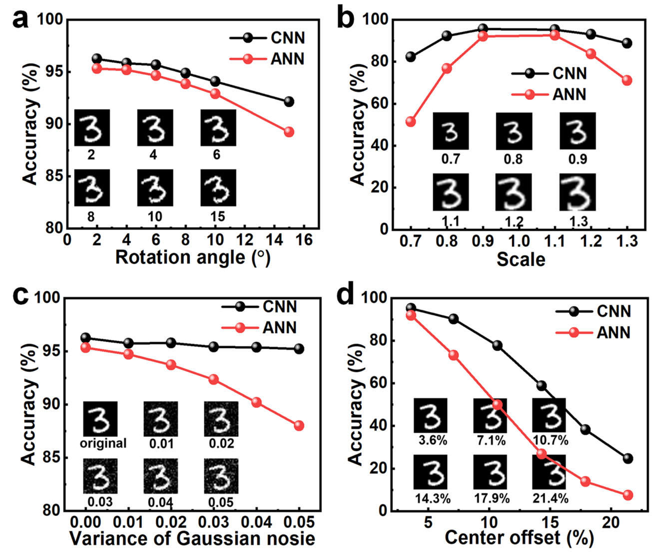

Fig. 5. (a) Image recognition accuracy versus different rotation angles. The inset shows pattern "3" with different angles and the numbers under patterns mean the degrees. (b), (c) and (d) are the image recognition accuracy versus scale, variance of Gaussian noise and center offset, respectively. The insets in each part are examples of different degrees.

To investigate the robustness of image recognition, Fig. 5 illustrates the impact of different interferences, including rotation (Fig. 5(a)), scale (Fig. 5(b)), Gaussian noise (Fig. 5(c)) and center offset (Fig. 5(d)). Fig. 5(a) and (b) show that a minor decrease in the accuracy of the CNN model is observed when the images were rotated from 0° to 15° and scaled from 0.7 to

1.3 times, respectively. For the same situation, the ANN model showed an unsatisfying performance. As shown in Fig. 5(c), with increasing variance of Gaussian noise, the recognition accuracy of CNN was slightly decreased, whereas relatively lower accuracy could be observed for the one using ANN model. When Gaussian noise with a variance of 0.05 is presented onto the digits, the overall accuracy still remains as high as 95.23% for CNN and only 88.01% for ANN. The results of this comparison indicate that CNN exhibits much better resistance to noise interference in this machine vision system [47], [48]. Fig. 5(d) shows that as the image offset increases from 3.57% to 21.34%, CNN accuracy drops from 95.1% to 24.55%, while ANN accuracy drops from 91.9% to 7.38%. The above experiments show that the center offset has the greatest impact on the detection accuracy and that the proposed CNN enabled machine vision system performs superior adaptability to objects rotation and scaling. The images scaling simulation indicates that the GaN NWs based machine vision system has potential to recognize the images with different sizes. These simulations also prove that CNN has higher accuracy and better robustness than ANN in the scenarios mentioned above. The reason for the superiority of CNN over ANN is that image characteristics and spatial information could be effectively extracted by convolutional kernels, whereas the image data in ANN is required to flatten into a one-dimensional form [49], [50]. Therefore, when the images are disturbed by interference, CNN could still detect the image characteristics and maintain a high accuracy rate. These results suggest that GaN NWs sensor array can effectively simplify the process of recognizing images and exhibits good immunity against interferences.

IV. Conclusion

A machine vision system based on a GaN NWs sensor array is developed in this article. High recognition accuracy and strong robustness in dim and noisy environments are achieved by taking advantage of the GaN NWs' high responsivity and low dark current, as well as applying appropriate machine learning algorithms. The recognition rates of normalization and binarization modes at varying light intensities are also investigated, proving that normalization is advantageous for complex images. Comparing the characteristics of ANN and CNN models in image recognition shows that CNN model with feature extraction is more robust in noise and low-light interference. Our work indicates that a high-performance image recognition system in UV environments could be implemented by exploiting outstanding properties of GaN NWs and applying CNN algorithm to boost immunity to interference.

References

[1] T. U. Rehman, M. S. Mahmud, Y. K. Chang, J. Jin, and J. Shin, "Current and future applications of statistical machine learning algorithms for agricultural machine vision systems," *Comput. Electron. Agriculture*, vol. 156, pp. 585–605, 2019.

[2] G. A. M. Meiring and H. C. Myburgh, "A review of intelligent driving style analysis systems and related artificial intelligence algorithms," *Sensors*, vol. 15, no. 12, pp. 30653–30682, 2015.

[3] J. Wang, P. Fu, and R. X. Gao, "Machine vision intelligence for product defect inspection based on deep learning and Hough transform," *J. Manuf. Syst.*, vol. 51, pp. 52–60, 2019.

[4] A. Dodda et al., "Bioinspired and low-power 2D machine vision with adaptive machine learning and forgetting," *ACS Nano*, vol. 16, no. 12, pp. 20010–20020, 2022.

[5] L. Mennel, J. Symonowicz, S. Wachter, D. K. Polyushkin, A. J. Molina-Mendoza, and T. Mueller, "Ultrafast machine vision with 2D material neural network image sensors," *Nature*, vol. 579, no. 7797, pp. 62–66, 2020.

[6] Q.-B. Zhu et al., "A flexible ultrasensitive optoelectronic sensor array for neuromorphic vision systems," *Nature Commun.*, vol. 12, no. 1, 2021, Art. no. 1798.

[7] D. Slaughter, D. Obenland, J. Thompson, M. Arpaia, and D. Margosan, "Non-destructive freeze damage detection in oranges using machine vision and ultraviolet fluorescence," *Postharvest Biol. Technol.*, vol. 48, no. 3, pp. 341–346, 2008.

[8] W. Li, Q. Lin, K. Wang, and K. Cai, "Machine vision-based network monitoring system for solar-blind ultraviolet signal," *Comput. Commun.*, vol. 171, pp. 157–162, 2021.

[9] G. J. Lee, C. Choi, D. H. Kim, and Y. M. Song, "Bioinspired artificial eyes: Optic components, digital cameras, and visual prostheses," *Adv. Funct. Mater.*, vol. 28, no. 24, 2018, Art. no. 1705202.

[10] S. Kim, G. Singh, Y. Jeong, S. Lee, and K. Lee, "Development of highly stable and sensitive SAW UV sensor based on Ta_2O_5 coated 1D ZnO/SnO_2 core–shell nanostructures," *Adv. Mater. Technol.*, vol. 8, no. 11, 2023, Art. no. 2201895.

[11] Z. Yang, J. Zhao, C. Liang, and H. Jiang, "Materials and device design for epidermal UV sensors with real-time, skin-color specific, and naked-eye quasi-quantitative monitoring capabilities," *Adv. Mater. Technol.*, vol. 8, no. 7, 2023, Art. no. 2201481.

[12] S. Dhar, P. Chakraborty, T. Majumder, and S. P. Mondal, "CdS-decorated al-doped ZnO nanorod/polymer schottky junction ultraviolet–visible dual-wavelength photodetector," *ACS Appl. Nano Mater.*, vol. 1, no. 7, pp. 3339–3345, 2018.

[13] P. E. Keivanidis, S.-H. Khong, P. K. Ho, N. C. Greenham, and R. H. Friend, "All-solution based device engineering of multilayer polymeric photodiodes: Minimizing dark current," *Appl. Phys. Lett.*, vol. 94, no. 17, 2009, Art. no. 173303.

[14] B. Chen, W. Jiang, J. Yuan, A. L. Holmes, and B. M. Onat, "SWIR/MWIR InP-based pin photodiodes with InGaAs/GaAsSb type-II quantum wells," *IEEE J. Quantum Electron.*, vol. 47, no. 9, pp. 1244–1250, Sep. 2011.

[15] A. S. Hastings, D. A. Tulchinsky, K. J. Williams, H. Pan, A. Beling, and J. C. Campbell, "Minimizing photodiode nonlinearities by compensating voltage-dependent responsivity effects," *J. Lightw. Technol.*, vol. 28, no. 22, pp. 3329–3333, Nov. 2010.

[16] A. Kumar, J. Ahuja, A. Mondal, and A. Bag, "Ga-In nanoparticle induced UV plasmonic impact on heterojunction based deep UV photodetector," *IEEE Trans. Nanotechnol.*, vol. 21, pp. 196–203, 2022.

[17] A. Mondal, S. Nandi, M. K. Yadav, A. Nandi, and A. Bag, "Broad range (254–302 nm) and high performance Ga_2O_3: SnO_2 based deep UV photodetector," *IEEE Trans. Nanotechnol.*, vol. 21, pp. 320–327, 2022.

[18] M. Tchernycheva et al., "Integrated photonic platform based on InGaN/GaN nanowire emitters and detectors," *Nano Lett.*, vol. 14, no. 6, pp. 3515–3520, 2014.

[19] Q. Liu et al., "Enhanced photoresponse of single GaN microwire ultraviolet photodetectors by heteroepitaxial AlN coating layer," *Adv. Mater. Technol.*, vol. 6, no. 8, 2021, Art. no. 2100226.

[20] P. Li et al., "Construction of GaN/Ga_2O_3 p–n junction for an extremely high responsivity self-powered UV photodetector," *J. Mater. Chem. C*, vol. 5, no. 40, pp. 10562–10570, 2017.

[21] Y. Yang et al., "Ultralow dark-current and superhigh detectivity ultraviolet photodetector based on freestanding GaN nanobelt array," *ACS Appl. Electron. Mater.*, vol. 4, no. 11, pp. 5421–5428, 2022.

[22] A. Dubey et al., "Aluminum plasmonics enriched ultraviolet GaN photodetector with ultrahigh responsivity, detectivity, and broad bandwidth," *Adv. Sci.*, vol. 7, no. 24, 2020, Art. no. 2002274.

[23] S. Cuesta et al., "Effect of bias on the response of GaN axial p–n junction single-nanowire photodetectors," *Nano Lett.*, vol. 19, no. 8, pp. 5506–5514, 2019.

[24] L. Rigutti et al., "Ultraviolet photodetector based on GaN/AlN quantum disks in a single nanowire," *Nano Lett.*, vol. 10, no. 8, pp. 2939–2943, 2010.

[25] M. Kumar, V. Kumar, and R. Singh, "Formation of ultralong GaN nanowires up to millimeter length scale and photoconduction study in single nanowire," *Scripta Materialia*, vol. 138, pp. 75–78, 2017.

[26] X. Wang et al., "Ultrafast, superhigh gain visible-blind UV detector and optical logic gates based on nonpolar a-axial GaN nanowire," *Nanoscale*, vol. 6, no. 20, pp. 12009–12017, 2014.

[27] A. K. Jain, J. Mao, and K. M. Mohiuddin, "Artificial neural networks: A tutorial," *Computer*, vol. 29, no. 3, pp. 31–44, 1996.

[28] Y. LeCun, L. Bottou, Y. Bengio, and P. Haffner, "Gradient-based learning applied to document recognition," *Proc. IEEE*, vol. 86, no. 11, pp. 2278–2324, Nov. 1998.

[29] F. Zhou et al., "Optoelectronic resistive random access memory for neuromorphic vision sensors," *Nature Nanotechnol.*, vol. 14, no. 8, pp. 776–782, 2019.

[30] X. Zou, X. Zhang, Y. Zhang, Q. Lyu, C. W. Tang, and K. M. Lau, "GaN single nanowire p–i–n diode for high-temperature operations," *ACS Appl. Electron. Mater.*, vol. 2, no. 3, pp. 719–724, 2020.

[31] S. D. Hersee, X. Sun, and X. Wang, "The controlled growth of GaN nanowires," *Nano Lett.*, vol. 6, no. 8, pp. 1808–1811, 2006.

[32] Q. Li et al., "Single-mode GaN nanowire lasers," *Opt. Exp.*, vol. 20, no. 16, pp. 17873–17879, 2012.

[33] K.-S. Im et al., "Fabrication of normally-off GaN nanowire gate-all-around FET with top-down approach," *Appl. Phys. Lett.*, vol. 109, no. 14, 2016, Art. no. 143106, doi: 10.1063/1.4964268.

[34] S. Zhang et al., "High responsivity GaN nanowire UVA photodetector synthesized by hydride vapor phase epitaxy," *J. Appl. Phys.*, vol. 128, no. 15, 2020, Art. no. 155705.

[35] S. Han, S. Noh, J.-W. Kim, C.-R. Lee, S.-K. Lee, and J. S. Kim, "Stretchable inorganic GaN-nanowire photosensor with high photocurrent and photoresponsivity," *ACS Appl. Mater. Interfaces*, vol. 13, no. 19, pp. 22728–22737, 2021.

[36] T. He et al., "Broadband ultraviolet photodetector based on vertical Ga_2O_3/GaN nanowire array with high responsivity," *Adv. Opt. Mater.*, vol. 7, no. 7, 2019, Art. no. 1801563.

[37] X. Zhou et al., "High-performance solar-blind deep ultraviolet photodetector based on individual single-crystalline Zn_2GeO_4 nanowire," *Adv. Funct. Mater.*, vol. 26, no. 5, pp. 704–712, 2016.

[38] Q. Feng et al., "$(AlGa)_2O_3$ solar-blind photodetectors on sapphire with wider bandgap and improved responsivity," *Opt. Mater. Exp.*, vol. 7, no. 4, pp. 1240–1248, 2017.

[39] B. Desiatov and M. Lončar, "Silicon photodetector for integrated lithium niobate photonics," *Appl. Phys. Lett.*, vol. 115, no. 12, 2019, Art. no. 121108.

[40] C. Huang et al., "Boosted ultraviolet photodetection of AlGaN quantum-disk nanowires via rational surface passivation," *J. Phys. D: Appl. Phys.*, vol. 55, no. 12, 2021, Art. no. 125101.

[41] W.-Y. Weng, T.-J. Hsueh, S.-J. Chang, S.-B. Wang, H.-T. Hsueh, and G.-J. Huang, "A high-responsivity GaN nanowire UV photodetector," *IEEE J. Sel. Topics Quantum Electron.*, vol. 17, no. 4, pp. 996–1001, Jul./Aug. 2011.

[42] R.-S. Chen et al., "Ultrahigh photocurrent gain in m-axial GaN nanowires," *Appl. Phys. Lett.*, vol. 91, no. 22, 2007, Art. no. 223106.

[43] X. Chen et al., "Analysis of the influence and mechanism of sulfur passivation on the dark current of a single GaAs nanowire photodetector," *Nanotechnology*, vol. 29, no. 9, 2018, Art. no. 095201.

[44] F. Liao et al., "Bioinspired in-sensor visual adaptation for accurate perception," *Nature Electron.*, vol. 5, no. 2, pp. 84–91, 2022.

[45] D. Beohar and A. Rasool, "Handwritten digit recognition of MNIST dataset using deep learning state-of-the-art artificial neural network (ANN) and convolutional neural network (CNN)," in *Proc. IEEE Int. Conf. Emerg. Smart Comput. Inform.*, 2021, pp. 542–548.

[46] Z. J. Wang et al., "CNN explainer: Learning convolutional neural networks with interactive visualization," *IEEE Trans. Vis. Comput. Graph.*, vol. 27, no. 2, pp. 1396–1406, Feb. 2021.

[47] M. Momeny, A. M. Latif, M. A. Sarram, R. Sheikhpour, and Y. D. Zhang, "A noise robust convolutional neural network for image classification," *Results Eng.*, vol. 10, 2021, Art. no. 100225.

[48] M. Hasan, S. Ullah, M. J. Khan, and K. Khurshid, "Comparative analysis of SVM, ANN and CNN for classifying vegetation species using hyperspectral thermal infrared data," *Int. Arch. Photogrammetry, Remote Sens. Spatial Inf. Sci.*, vol. 42, pp. 1861–1868, 2019.

[49] D. S. Prashanth, R. V. K. Mehta, and N. Sharma, "Classification of handwritten Devanagari number–An analysis of pattern recognition tool using neural network and CNN," *Procedia Comput. Sci.*, vol. 167, pp. 2445–2457, 2020.

[50] T. B. Alakus and I. Turkoglu, "Comparison of deep learning approaches to predict COVID-19 infection," *Chaos, Solitons Fractals*, vol. 140, 2020, Art. no. 110120.